Mechanics & Industry **16**, 203 (2015)

DOI: 10.1051/meca/2014085
www.mechanics-industry.org

Mechanics & Industry

A parametric study on the performance of a Ranque-Hilsch vortex tube using a CFD-based approach

Nader Pourmahmoud[1], Ashkan Feyzi[1], Ali Atashbar Orang[2] and Amin Paykani[2,a]

[1] Department of Mechanical Engineering, Urmia University, Urmia, Iran
[2] Young Researchers and elite Club, Tabriz Branch, Islamic Azad University, Tabriz, Iran

Received 23 July 2014, Accepted 8 October 2014

Abstract – In this paper, a numerical investigation is carried out to realize the behavior of a fabricated vortex tube. A computational fluid dynamics model is used to simulate the flow field structure in the tube in order to study the effects of various parameters on the performance and temperature separation. Numerical results such as temperature separation versus cold outlet mass fraction are obtained for a specific vortex tube with given inlet thermo physical properties. The numerical results are obtained for various amounts of cold outlet mass fractions. The calculated temperature distributions inside the Ranque-Hilsch Vortex Tube (RHVT) are simultaneously compared with available experimental results and a good agreement between them is noticed. It is found that increasing the inlet nozzle height improves the performance of the RHVT. The results also indicated that small values of cold mass fraction give best result in cold exit temperature difference.

Key words: Ranque-Hilsch vortex tube / cold mass fraction / temperature difference / temperature distribution / pressure distribution

Nomenclature

ρ	Density (kgm^{-3})
μ	Dynamic viscosity (kg.m^{-1}.s^{-1})
μ_t	Turbulent viscosity (kg.m^{-1}.s^{-1})
K	Conductivity coefficient (W.m^{-1}.K^{-1})
c_p	Specific heat at constant pressure (J.kg^{-1}.K^{-1})
R	Specific constant of an ideal gas
Pr	Prandtl number
p	Pressure (Pa)
T	Static temperature (K)
δ_{ij}	Kronecker delta
τ_{ij}	Stress tensor components

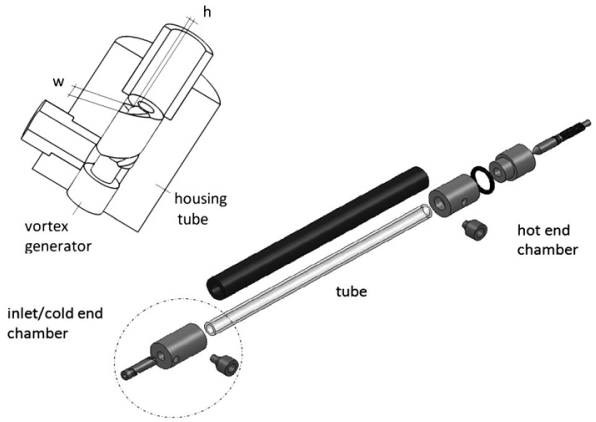

Fig. 1. Schematic drawing of the Vortex tube system.

1 Introduction

Ranque-Hilsch vortex tube is a simple device with non-moving parts, which is capable of separating a high-pressure gas flow into two lower pressure flows of different temperatures. As shown in Figure 1, this phenomenon is occurred when compressed air flows tangentially into the vortex chamber through the inlet nozzles. The device is consisted of a simple circular tube, with one or more azimuthally nozzles for flow inlet and two outlets for separated flow exits. High pressure air enters the tube azimuthally at one end and produces a strong vortex flow in the tube. Then, the gas expands through the nozzle and achieves a high angular velocity, causing a vortex-type flow in the tube. Separating cold and hot airs by using the principles of the vortex tube, can be applied to industrial applications such as cooling equipment in CNC machines, refrigerators, cooling suits, heating processes, etc. The vortex tube is well-suited for these applications because it is simple, compact, light, quiet, and does not use freon or other refrigerants (CFCs/HCFCs). They are popular for their reliability (having non-moving

[a] Corresponding author: a.paykani@gmail.com

parts), lack of maintenance and simple and inexpensive construction.

There are two exits to the tube: the hot exit is placed near the outer radius of the tube at the end away from the nozzle, and the cold exit is placed at the center of the tube at the nozzle's chambers. The gas is separated into two streams, one at higher and the other at lower temperature than the inlet gas temperature. This effect is referred to as the temperature separation effect that reported for the first time by Ranque in 1931 when he was studying processes in a dust separation cyclone [1]. His design of the vortex tube has later been improved by the German physicist [2], who arranged a diaphragm at the cold gas side. He suggested that angular velocity gradients in the radial direction rises frictional coupling between different layers of the rotating flow. Thus, the migration of energy via shear work would occur from the inner layers to the outer ones. Other investigators have attributed the energy separation to work transfer via compression and expansion. Several variations of this theory are described in the literature, varying according to the mechanism driving the fluid motion. Harnett and Eckert [3] invoked turbulent eddies; Ahlborn and Gordon [4] described an embedded secondary circulation. Stephan et al. [5] proposed the formation of Gortler vortices on the inside wall of the vortex tube that drive the fluid motion. Kurosaka [6] reported the temperature separation as a result of acoustic streaming effect that transfers energy from the cold core to the hot outer annulus. Gutsol [7] hypothesized the energy separation to be a consequence of the interaction of micro volumes in the vortex tube. Despite all the proposed theories, none has been able to explain the temperature separation effect satisfactorily.

Recent efforts have successfully utilized computational fluid dynamics (CFD) modeling to explain the fundamental principles behind the energy separation produced by the vortex tube. Frohlingsdorf and Unger [8] modeled the flow within a vortex tube using a CFD solver that included compressible and turbulence effects. The numerical predictions qualitatively predicted the experimental results presented by Bruun [9]. Ahlborn et al. [10, 11] indicated the dependence of vortex tube performance on normalized pressure drop with a numerical model. Aljuwayhel et al. [12] employed a fluid dynamics model of the vortex tube to understand the process that drives the temperature separation phenomena. They reported that the energy separation exhibited by the vortex tube is due to the work transfer caused by a torque produced by viscous shear acting on a rotating control surface, which separates the cold flow region and the hot flow region. Skye et al. [13] used a model similar to that of [12]. They also measured the inlet and outlet temperatures of the vortex tube and compared with the predictions from the fluid dynamics model. The temperature separation predicted by their model for commercially available vortex tube was found to be in reasonable agreement to the experimental measurements. Akhesmeh et al. [14] carried out a computational fluid dynamics analysis in order to predict the flow fields and the associated temperature separation within a Ranque-Hilsch vortex tube. Simulations were carried out for varying amounts of cold outlet mass flow rates. Shamsoddini et al. [15, 16] investigated the effects of the nozzles number on the flow and power of cooling of a vortex tube using a three-dimensional CFD model. They showed that as the number of nozzles is increased, power of cooling increases while cold outlet temperature decreases. The further expounded the correlations for the velocity magnitude to the normal velocity using CFD. They indicated that the proposed method is a proper one for optimization of cooling performance of a vortex tube. Pourmahmoud et al. [17,18] investigated the effect of length to diameter ratio on the fluid flow characteristics and energy separation phenomenon inside the Ranque-Hilsch vortex tube. The results indicated that the temperature difference between hot and cold gas flow can be improved by increasing the length of vortex tube such that stagnation point is located far from the nozzle inlet and within the tube. They conducted another research work to study the effect of helical nozzles on both energy separation and refrigeration phenomena in the Ranque-Hilsch Vortex Tube by CFD techniques. They found that temperature separation was increased due to increase of nozzle numbers; however the coefficient of performance (COP) does not change significantly. Avci [19] carried out an experimental study to investigate the effects of nozzle aspect ratio and nozzles number on the performance of a vortex tube. The obtained results revealed that the nozzle aspect ratio has a great effect on the energy/temperature separation mechanism. The results also showed that the vortex tube with a single nozzle yields better performance than the vortex tube with 2 and 3 nozzles.

A few experimental and numerical parametric studies have been conducted in recent years on performance of a vortex tube. In the present study, since the flow field inside the vortex tube is assumed to be axisymmetric and steady state, only a section of tube is taken into account for analysis with cyclic boundary condition. The standard k-ε turbulence model is applied to the compressible Navier-Stokes equations for numerical analyzing of computational domain. Discretizing of derivatives terms is performed using second order upwind along with Quick numerical schemes, respectively. It has been used to simulate the flow patterns and temperature separation phenomenon in a Ranque-Hilsch vortex tube (RHVT), which has two convergent circumferential nozzles. Numerical results such as temperature separation versus cold outlet mass fraction are obtained for a specific vortex tube with given inlet thermo physical properties. Moreover, an experimental investigation is conducted to validate the numerical results. Both numerical and experimental results are obtained for various amounts of cold outlet mass fractions.

2 Theoretical analysis

Flow is assumed compressible and turbulent and governing equations for fluid flow and heat transfer are as follows:

Continuity equation:

$$\frac{\partial}{\partial x_i}(\rho u_i) = 0 \tag{1}$$

Momentum equations:

$$\frac{\partial}{\partial x_j}(\rho u_i u_j) = -\frac{\partial p}{\partial x_i} + \frac{\partial}{\partial x_j}\left[\mu\left(\frac{\partial u_i}{\partial x_j} + \frac{\partial u_j}{\partial x_i} - \frac{2}{3}\delta_{ij}\frac{\partial u_k}{\partial x_k}\right)\right] + \frac{\partial}{\partial x_j}(-\overline{\rho u_i} u_j) \tag{2}$$

Energy equation:

$$\frac{\partial}{\partial x_i}\left[u_{i\rho}\left(h + \frac{1}{2}u_j u_j\right)\right] = \frac{\partial}{\partial x_j}\left[k_{\text{eff}}\frac{\partial T}{\partial x_j} + u_i(\tau_{ij})_{\text{eff}}\right],$$

$$k_{\text{eff}} = K + \frac{c_p \mu_t}{Pr_t} \tag{3}$$

The first term on the left hand side of the energy equation represents the rate of total energy of the fluid element lost by convection; the first and second terms on the right-hand side of it represent conduction energy transfer and viscous dissipation, respectively. It is noted that summation rule is used for repeated indices: i and j.
State equation for an ideal gas:

$$p = \rho R T \tag{4}$$

Flow in the vortex tube is highly turbulent. The steady state assumption and practical considerations indicate that a turbulence model must be employed to represent its effects. The turbulence kinetic energy, k, and its rate of dissipation, ε are obtained from the following transport equations:

$$\frac{\partial}{\partial t}(\rho k) + \frac{\partial}{\partial x_i}(\rho k u_i) = \frac{\partial}{\partial x_i}\left[\left(\mu + \frac{\mu_t}{\sigma_k}\right)\frac{\partial k}{\partial x_j}\right] + G_k + G_b - \rho\varepsilon - Y_M \tag{5}$$

$$\frac{\partial}{\partial t}(\rho k) + \frac{\partial}{\partial x_i}(\rho k u_i) = \frac{\partial}{\partial x_j}\left[\left(\mu + \frac{\mu_t}{\sigma_\varepsilon}\right)\frac{\partial \varepsilon}{\partial x_j}\right] + G_{1\varepsilon}\frac{\varepsilon}{k}(G_k + C_{3\varepsilon}G_b) - C_{2\varepsilon}\rho\frac{\varepsilon^2}{k} \tag{6}$$

In these equations, G_k represents the generation of turbulent kinetic energy due to the mean velocity gradients, G_b is the generation of turbulence kinetic energy due to buoyancy that is neglected. Y_M denotes the contribution of the fluctuating dilatation in compressible turbulence to the overall dissipation rate, and finally $C_{1\varepsilon}$, $C_{2\varepsilon}$, and $C_{3\varepsilon}$ are constants values. σ_ε and σ_k are the turbulent Prandtl numbers for k and ε, respectively. The turbulent (or eddy) viscosity, μ_t, is computed by combining k and ε as follows:

$$\mu_t = \rho C_\mu \frac{k^2}{\varepsilon} \tag{7}$$

where, C_μ is a constant.

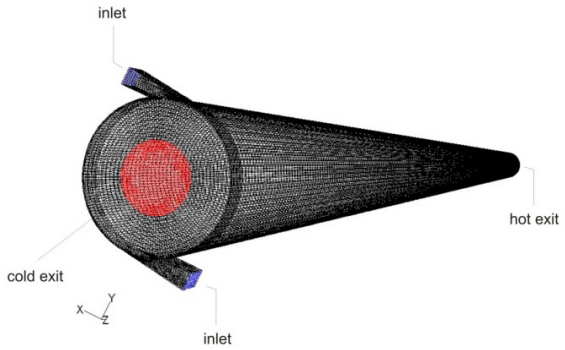

Fig. 2. Three-dimensional CFD model of vortex tube.

3 Numerical modeling of vortex tube

The numerical modeling of the vortex tube has been carried out using CFD package FLUENT (version: 6.3.26). The flow is assumed as 3-D, steady-state and employs the standard k-ε turbulence model. According to the three-dimensional computational domain shown in Figure 2, Finite Volume Method with a three-dimensional mesh is used and the boundary conditions are applied. Basic assumptions for all the computations of the particular vortex-tube flows are made as following: two circumferential pressurized gas inlets and two axial orifices for cold and hot stream, supersonic flow inside the vortex tube and ideal gas (arbitrary air). Since the model is consisted of two convergent nozzles, the CFD model is assumed to be a rotational periodic flow and only a sector of the flow domain with angle 180° needs to be considered throughout and special treatment for the flow at the inlet must be made for the computations. The diameter of the vortex tube is set to 8.5 mm, the width of the slot at the nozzle exhaust is fixed to 1 mm, whereas the length of the tube and the height of the nozzle slot are different in different cases, respectively. The cold and hot exits are axial orifices, the cold exit diameter is fixed at 4 mm and the hot exit area is the governing factor to achieve expected cold mass fractions.

For all cases in this analysis, the simulation boundary conditions for the model were identified based on the experimental measurements by Skye [13]. The inlet is modeled as a mass flow inlet. The specified total mass flow rate and stagnation temperature were fixed to 8.35 g.s^{-1} and 294.2 K, respectively. The static pressure at the cold exit boundary was fixed at experimental measurements pressure. The static pressure at the hot exit boundary is adjusted in the way to vary the cold mass fraction.

3.1 Grid dependence study

To remove the errors due to coarseness of grids, analysis has been carried out for different average unit cell volumes in the optimized vortex tube with $L = 270$ mm, $h = 2$ mm and $\alpha = 0.2$. The variation of total temperature difference and maximum swirl velocity as key parameters are shown in Figures 3 and 4 for different unit

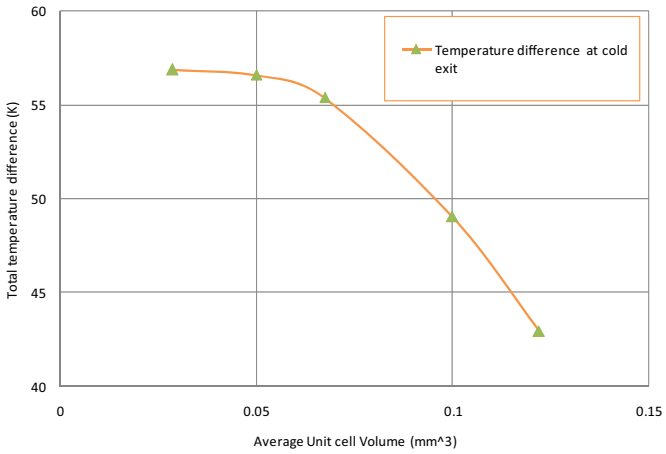

Fig. 3. Grid size dependence study on total temperature difference at different average unit cell volumes.

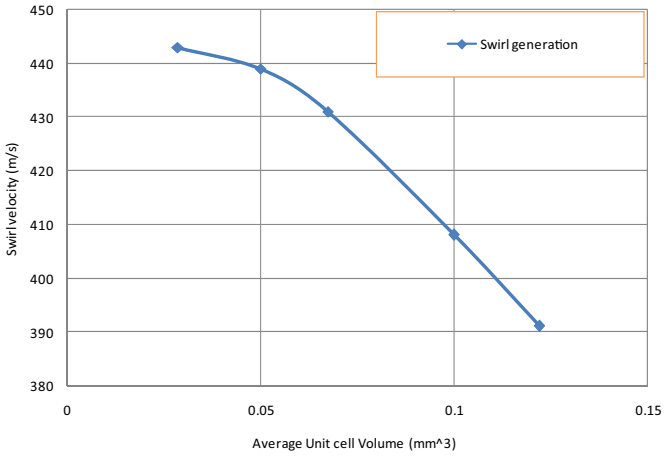

Fig. 4. Grid size dependence study on maximum swirl velocity at different average unit cell volumes.

Table 1. The geometrical information of different cases.

	L (mm)	w (mm)	h (mm)	d_c (mm)	α	N_{in}
Case 1	135	1	1	4	0.2	2
Case 2	270	1	1	4	0.2	2
Case 3	350	1	1	4	0.2	2

Table 2. The maximum temperature variations obtained for different tube lengths; compared with experimental data [13].

	Result	L (mm)	ΔT (K)	ΔT_h (K)	ΔT_c (K)	Max temp. separation (K)
Case 1	CFD	135	17.91	12.15	–5.76	46.98
	Experiment	135	19.00	12.89	–6.11	49.85
Case 2	CFD	270	23.96	14.99	–8.96	47.17
	Experiment	270	24.94	15.61	–9.33	49.11
Case 3	CFD	350	22.53	15.84	–6.69	44.39
	Experiment	350	25.011	17.59	–7.42	49.27

cell volumes, respectively. It can be seen that there is no much advantage in reducing the unit cell volume size below 0.0286 mm^3 corresponding to 0.296 million cells for the studied configuration.

4 Validation

4.1 The effect of tube length

Three different tube lengths (135 mm, 270 mm and 350 mm) have been investigated. The main characteristics of the geometry of the systems are indicated in Table 1. The obtained results are compared with the experimental and computational results in reference [13], that both models have similar geometry and boundary conditions.

Table 2 shows the maximum temperature variations obtained for three different lengths. When the tube length is increased from 135 mm up to 270 mm, the maximum obtained temperature (ΔT) increases, thus, the performance improves, but for the increases from 270 mm up to 350 mm, the maximum obtained temperature (ΔT) decreases, where $\Delta T = T_h - T_c$, $\Delta T_h = T_h - T_{in}$ and $\Delta T_c = T_c - T_{in}$. So we choose $L = 270$ mm as the optimum tube length. The simulated ΔT_h at both models are close to the experimental results.

The results of comparison between experimental and numerical results under the same operating conditions are illustrated in Figure 5.

4.2 The effect of inlet nozzle

In order to study the influence of inlet nozzles, according to Table 3, three different nozzle slot heights (1, 1.5 and 2 mm) have been investigated for the vortex tube with fixed tube length of $L = 270$ mm. The results of this study are given in Table 4.

As can be seen from Table 4, as the nozzle slot height increases from 1 mm up to 2 mm, the cold exit temperature difference (ΔT_c) and maximum temperature difference (ΔT) increase, so the performance improves. Consequently we select $h = 2$ mm as the optimum slot height

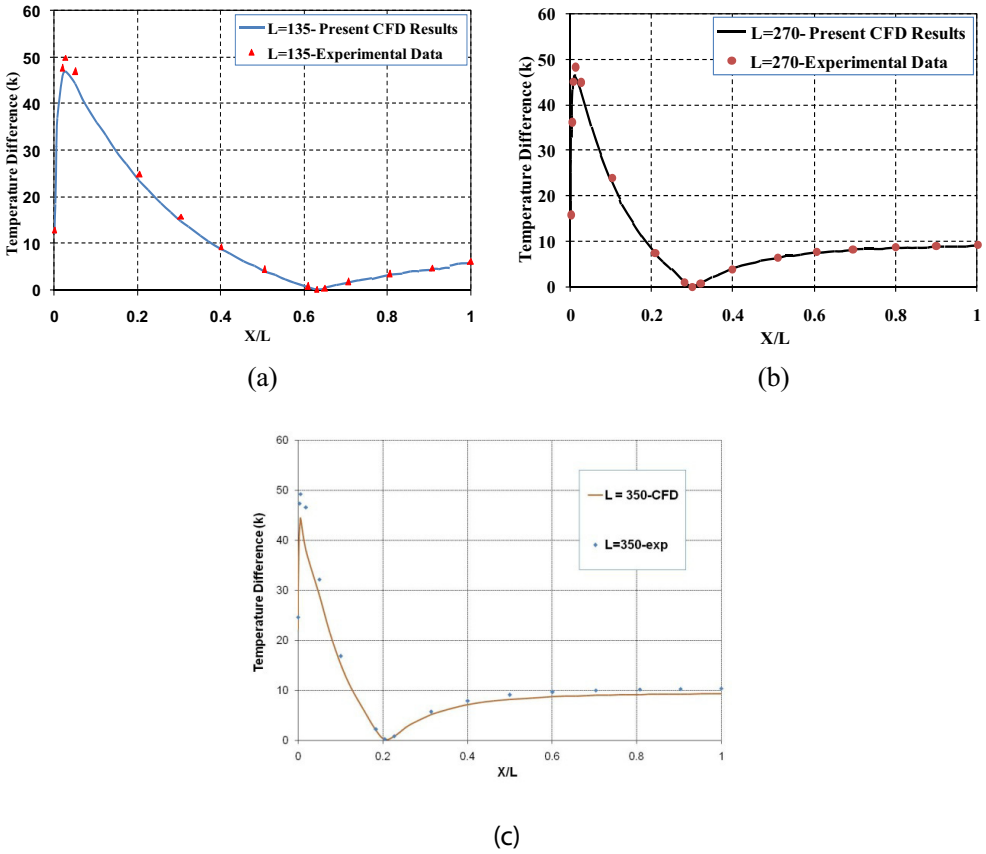

Fig. 5. Comparison between experimental [13] and numerical results for different tube lengths: (a) $L = 135$ mm; (b) $L = 270$ mm; (c) $L = 350$ mm.

Table 3. The geometrical information of different cases to study the influence of inlet nozzle.

	L (mm)	w (mm)	h (mm)	d_c (mm)	α	N_{in}
Case 1	270	1	1	4	0.2	2
Case 2	270	1	1.5	4	0.2	2
Case 3	270	1	2	4	0.2	2

Table 4. The maximum temperature differences obtained for different nozzle heights; compared with experimental data [13].

	Result	h (mm)	ΔT (K)	ΔT_h (K)	ΔT_c (K)	Max temp. separation (K)
Case 1	CFD	1	23.96	8.96	–15.00	46.20
	Experiment	1	25.52	9.55	–15.97	49.20
Case 2	CFD	1.5	56.07	9.78	–46.28	49.96
	Experiment	1.5	58.64	10.23	–48.41	52.26
Case 3	CFD	2	60.15	8.69	–51.46	56.61
	Experiment	2	64.72	9.35	–55.37	60.91

which results in best temperature difference and continue our investigations with the optimized tube length and nozzle height.

The comparisons between experimental and numerical results are shown in Figure 6. The temperature difference plots show a decrease of its values towards the periphery. Also, temperature difference increases with increasing of tube length especially at longer models.

4.3 The effect of cold mass fraction (α)

The influence of the cold mass fraction has also been investigated numerically and experimentally in the present study. Since we considered the optimum tube length and the nozzle slot height to be constant; hence, we studied the effect of the cold mass fraction variation on the temperature separation. The main characteristics of the geometry of the cases are indicated in Table 5.

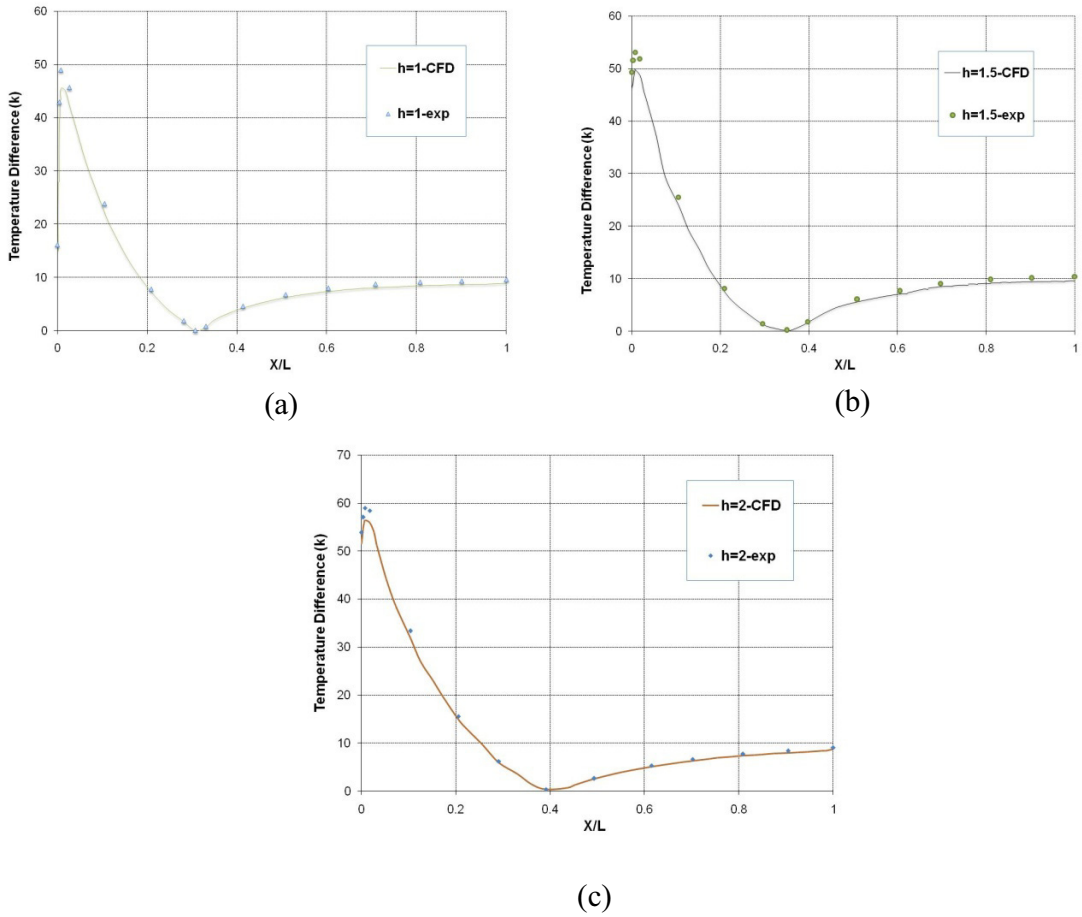

Fig. 6. Comparison between experimental [13] and numerical results for different nozzle heights: (a) $h = 1$ mm; (b) $h = 1.5$ mm; (c) $h = 2$ mm.

Table 5. The geometrical information of different cases to study the influence of cold mass fraction.

	L (mm)	w (mm)	h (mm)	d_c (mm)	α	N_{in}
Case 1	270	1	2	4	0.2	2
Case 2	270	1	2	4	0.35	2
Case 3	270	1	2	4	0.5	2
Case 4	270	1	2	4	0.65	2
Case 5	270	1	2	4	0.8	2

It can be concluded from Table 6 that the maximum cold exit temperature difference can be obtained for $\alpha = 0.2$, and as the cold mass fraction increases from 0.2 up to 0.8, the cold exit temperature difference decreases reciprocally.

Figure 7 shows the results for the above cases under the same operating conditions and the comparison between experimental and numerical results. The significant disagreement with the experimental data in Figures 7b and 7c is because of the fact that the boundary condition for the temperature was set through the inside of computational domain, but since the computational space (grid) was low in the nozzle and the flow could not develop completely, so the boundary condition may not work efficiently and numerical oscillations would be generated. Figure 8 demonstrates the temperature distribution contours in a longitudinal cross section of tube for different cold mass fractions. It is evident that for lower α, the temperature difference is dropped reaching 0 at $x/L = 0.42$, but then it increases to higher values. For higher α, the x/L that temperature difference becomes zero is reduced and after that point the temperature difference is greatly increased.

5 Results and discussions

5.1 The effect of stagnation point

The results of present study show that the performance of vortex tubes is related to stagnation point location. Furthermore, study on the tube length effect is required to explore the stagnation point location along the tube to acquire the highest energy separation. The stagnation point position within the vortex tube can be established from the velocity profile along the tube length at the point where axial velocity ceases to have a negative value. Also, it can be established according to the

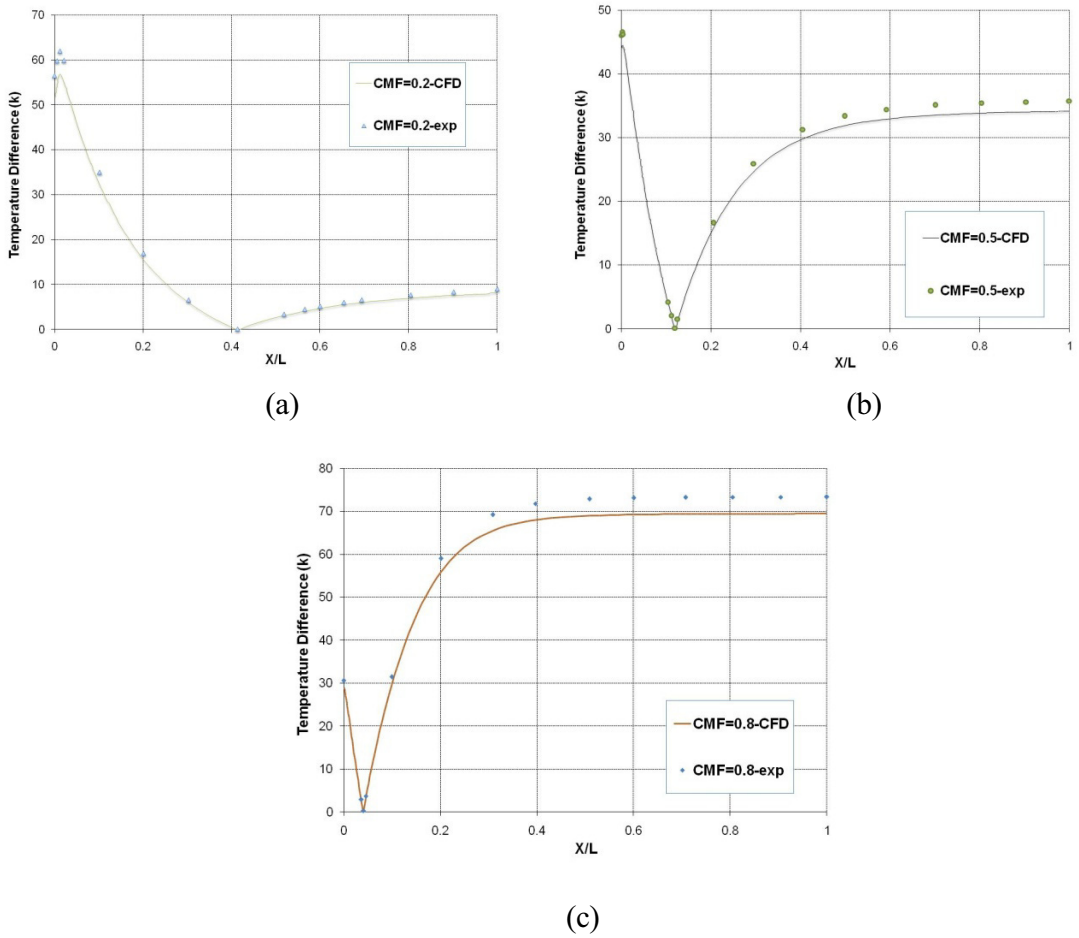

Fig. 7. Comparison between experimental [13] and numerical results for different cold mass fractions: (a) $\alpha = 0.2$; (b) $\alpha = 0.5$; (c) $\alpha = 0.8$.

Table 6. The maximum temperature differences obtained for different cold mass fractions. Compared with experimental data [13].

	Result	α	ΔT (K)	ΔT_h (K)	ΔT_c (K)	Max temp. separation (K)
Case 1	CFD	0.2	60.13	8.24	–51.89	56.89
	Experiment	0.2	65.48	8.98	–56.50	61.94
Case 2	CFD	0.35	68.12	19.03	–47.61	50.03
	Experiment	0.35	74.05	20.68	–51.75	54.38
Case 3	CFD	0.5	78.30	34.22	–44.07	44.47
	Experiment	0.5	81.82	35.77	–46.05	46.47
Case 4	CFD	0.65	89.36	46.11	–35.57	56.94
	Experiment	0.65	94.18	48.60	–37.49	60.02
Case 5	CFD	0.8	98.42	69.46	–28.96	69.46
	Experiment	0.8	103.93	73.35	–30.58	73.35

maximum wall temperature, where this point represents the stagnation point described by Fulton [18]. It was assumed that the wall temperature was representative of the gas temperature that reported by Frohlingsdorf and Unger [8]. Therefore, we measured the wall temperature along the tube length in different positions at the optimum tube length of $L = 270$ mm, for various inlet pressures including $p = 5$, 6 and 7 bar, and then collected the same types of data through numerical simulation models.

The variations of axial velocity along the center line of the vortex tube are shown in Figure 9 where the Z/L is represented as the dimensionless length of vortex tube. As indicated in this Figure, there is an axial distance between cold and hot ends that the velocity magnitude reaches to zero. This point is specified as the stagnation point position. Also, it can be inferred from Figure 9a that the stagnation point moves closer to the hot end as the inlet pressure increases.

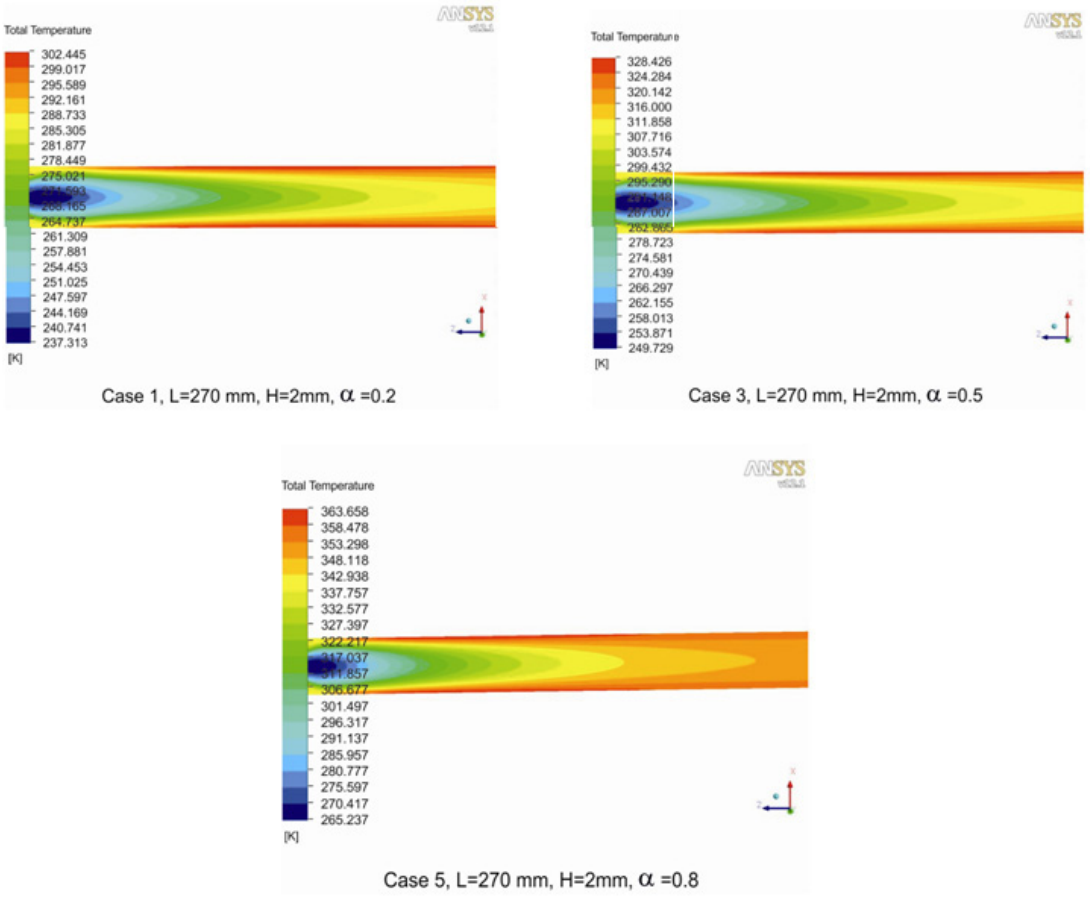

Fig. 8. Temperature distribution counters for different cases.

5.2 The effect of number of nozzles

In order to study the effect of type of inlet nozzle, three different arrangements of nozzles are simulated, having 2, 3 and 6 intakes, with constant inlet cross-sectional area. Variation of the cold and hot air and total temperature difference versus the cold mass ratio are shown in Figure 10. As the number of nozzles increases, flow in the main tube becomes more turbulent due to more interactions of injected flows. Therefore, the energy and temperature separation and consequently cold temperature difference and efficiency increase. The result is that the chamber with six intakes shows better performance than two and three-intake nozzle from refrigeration efficiency viewpoint.

Furthermore, it is important to have a high peripheral velocity in the portion of the tube immediately after the nozzle to achieve the best energy separation and performance inside the vortex tube. So, we have measured peripheral velocity shown in Figure 11 through our numerical modeling. Results of this Figure illustrated that the peripheral velocity in the portion of the tube immediately after the nozzle increases while the number of inlet nozzles increases. Hence, increasing of the number of nozzles enhances swirl velocity inside the vortex tube chamber leading to the increasing of energy separation.

Correlation between the swirl velocity and temperature difference has been demonstrated in all of previous research of vortex tube. Subsequently, numerical values of temperature distribution in different cross sections of tube are shown in Figure 12. It depicts the mentioned correlation of swirl velocity and temperature counters. The obtained results in this case are based on six-inlet nozzle with maximum swirl velocity equal to 449 ($\mathrm{m\,s^{-1}}$).

Total temperature difference for the different number of inlet nozzles throughout vortex tube length is illustrated in Figure 13.

For quick summery and comprehensive realizing of cold mass fraction and number of nuzzles effect, the numerical results are gathered in Table 7. It is clear that maximum energy separation and swirl velocity are attained in $\alpha = 0.2$ and in the chamber with six nozzles inlet. The economical power consumption to supply high pressure gas for operation of vortex tube is important as well as our goal of producing maximum cold temperature difference. Vortex tube with six number of nozzle inlets apparently produces maximum cold temperature difference. But it should be noted that power consumption is also increased intensively. Hence, it is recommended to use the vortex tube with 2 or maximum 3 number of nozzles, while the cold mass fraction in all cases must be fixed to 0.2.

Takahama [20] suggested using of a tube length $L \geqslant 100D_{vt}$ in order to obtain a better performance. In references [5–7], the tube length was suggested to be longer

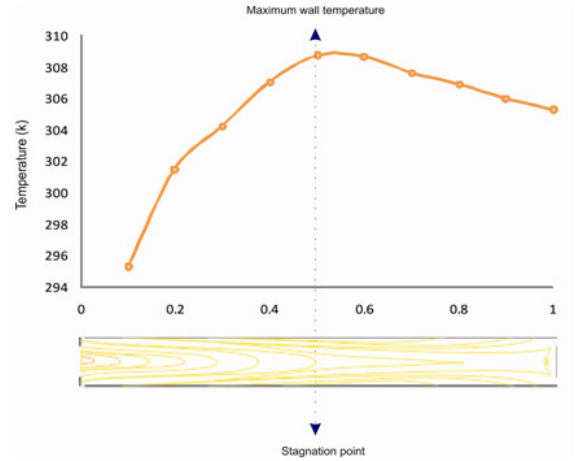

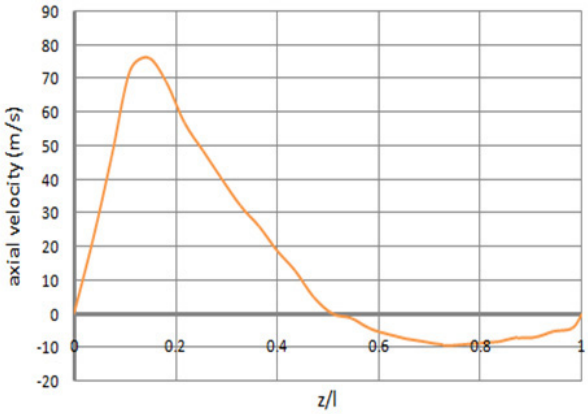

(a)

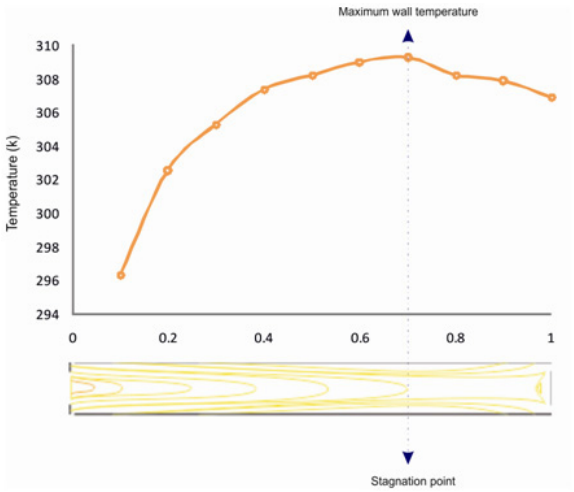

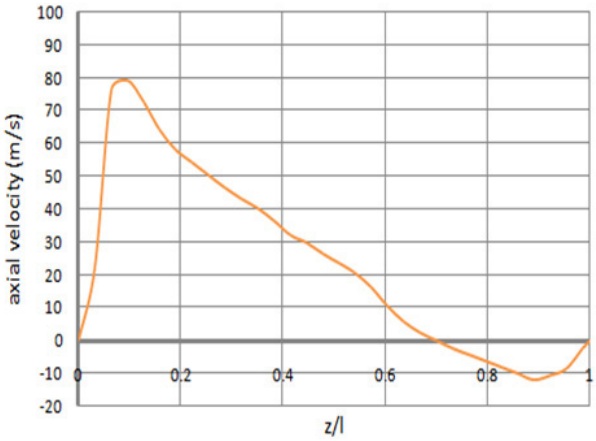

(b)

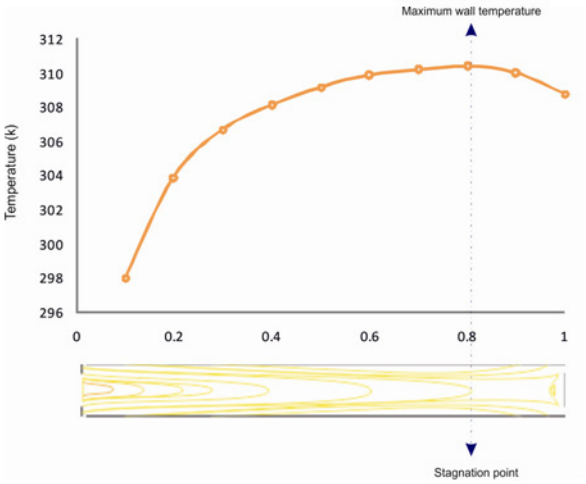

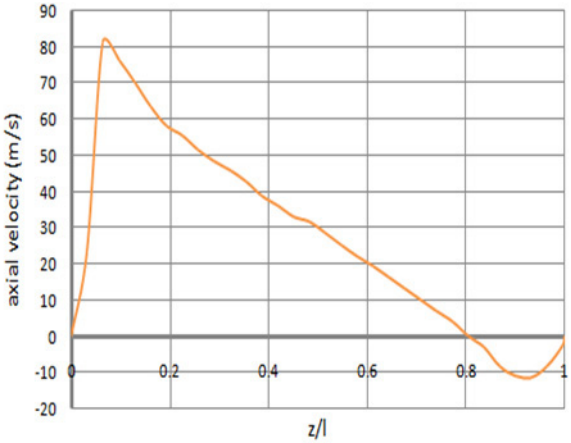

(c)

Fig. 9. Wall temperature and axial velocity curves: (a) $p = 5$ bar; (b) $p = 6$ bar; (c) $p = 7$ bar.

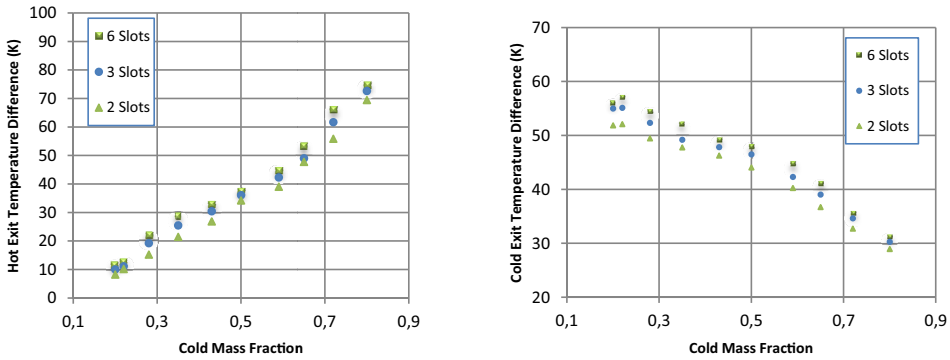

(a) (b)

Fig. 10. The effect of the cold mass ratio for the different number of inlet nozzles: (a) on the hot air temperature difference; (b) on the cold air temperature difference.

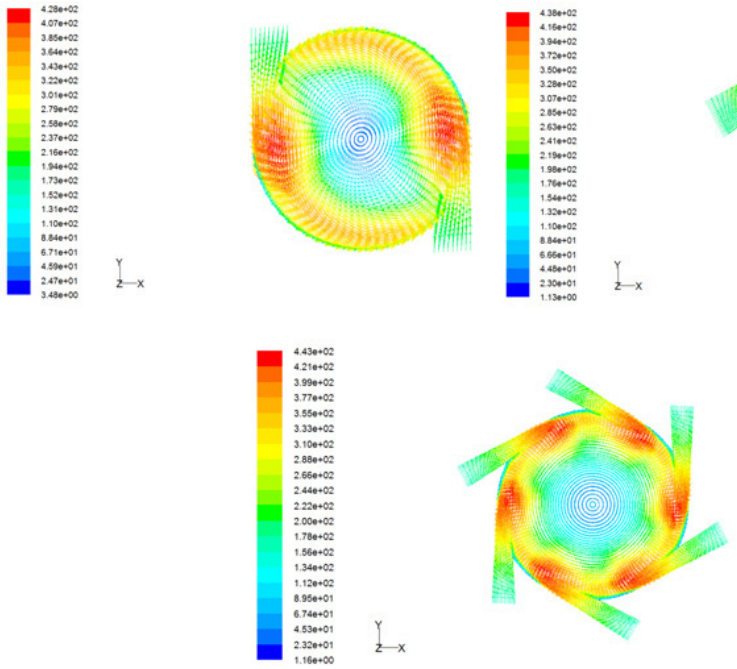

Fig. 11. Velocity counters for vortex tube with different number of inlet nozzles.

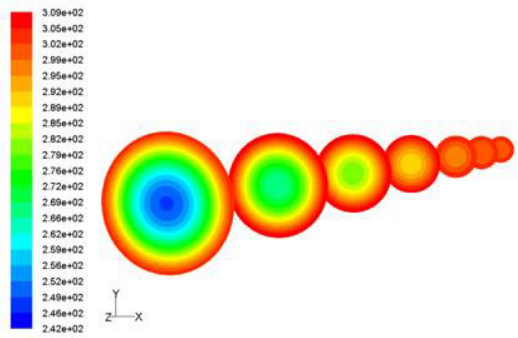

Fig. 12. Temperature distribution in different cross sections of tube.

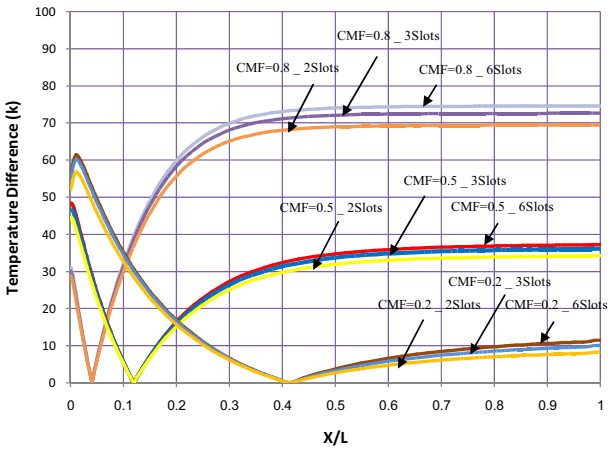

Fig. 13. Total temperature difference for the different number of inlet nozzles throughout vortex tube length.

Table 7. The comparison of temperature separation and maximum peripheral velocity in vortex tubes with different number of nozzles.

Cold mass fraction α	Number of Nozzle	ΔT (K)	ΔT_h (K)	ΔT_c (K)	Max Velocity (m.s^{-1})
0.2	2	60.13	8.24	51.89	443
	3	65.06	10.06	55.00	446
	6	67.49	11.46	56.03	449
0.5	2	78.30	34.23	44.07	428
	3	82.60	36.11	46.49	430
	6	85.19	37.24	47.95	433
0.8	2	98.42	69.46	28.96	412
	3	102.95	72.65	30.29	416
	6	105.70	74.60	31.11	420

than $45D_{vt}$. In this letter, the results of the study suggested that a tube length of 270 mm is optimal corresponding to L/D_{vt} about 32 (increasing of L/D_{vt} up to 41 obtained cold exit temperature difference decreasing). The effect of the inlet nozzle height is very clear. Increasing the inlet nozzle height improves the performance of the RHVT. The measured results with different cold mass fractions suggested that small values of this parameter give best results in cold exit temperature difference. In summary, the tube length, the geometry of the nozzle (type and sizes) and the cold mass fraction are important parameters.

6 Conclusions

In this paper, numerical study has been carried out to predict compressible vortex tube flow. Axisymmetric geometry and steady state flow assumptions were taken into account. Simulations were conducted for different tube lengths, nozzle heights and cold mass fractions by changing the hot exit area. The effects of tube length, nozzle height and cold mass fraction on the temperature separation were studied and the optimized values for these parameters were determined. The cold mass fraction was varied by varying the hot exit area. The general trends of the total temperature separations (hot and cold exit) predicted by the model were found to be in good agreement with the experimental results. Furthermore, it was suggested to utilization of the vortex tube with 2 or maximum 3 number of nozzles, while the cold mass fraction in all cases was fixed to 0.2.

References

[1] G.J. Ranque, Experiences sur la détente giratoire avec simultanéite d'un échappement d'air chaud et d'un échappement d'air froid, Journal de Physique et le Radium 4 (1933) 112–114

[2] R. Hilsch, Die expansion von gasen im zentrifugalfeld als kälteproze, Z. Naturforschung 1 (1946) 208–214

[3] J. Harnett, E. Eckert, Experimental study of the velocity and temperature distribution in a high velocity vortex-type flow, Trans. ASME 79 (1957) 751–758

[4] B. Ahlborn, J. Gordon The vortex tube as a classical thermodynamic refrigeration cycle, J. Appl. Phys. 88 (2000) 3645–653

[5] K. Stephan, S. Lin, M. Durst, F. Huang, D. Seher, An investigation of energy separation in a vortex tube, Int. J. Heat Mass Transfer 26 (1983) 341–348

[6] M. Kurosaka, Acoustic streaming in swirling flows, J. Fluid Mech. 124 (1982) 139–172

[7] A.F. Gutsol, The Ranque effect, Phys. Uspekhi 40 (1997) 639–658

[8] W. Frohlingsdorf, H. Unger, Numerical investigations of the compressible flow and the energy separation in the Ranque-Hilsch vortex tube, Int. J. Heat Mass Transfer 42 (1999) 415–422

[9] H.H. Bruun, Experimental investigation of the energy separation in vortex tubes, J. Mech. Eng. Sci. 11 (1969) 567–582

[10] B. Ahlborn, J.U. Keller, R. Staudt, G. Treitz, R. Rebhan, Limits of temperature separation in a vortex tube, J. Phys. D 27 (1994) 480–488

[11] B. Ahlborn, J. Camire, J.U. Keller, Low pressure vortex tubes, J. Phys. D 29 (1996) 1469–1472

[12] N.F. Aljuwayhel, G.F. Nellis, S.A. Klein, Parametric and internal study of the vortex tube using a CFD model, Int. J. Refrig. 28 (2005) 442–450

[13] H.M. Skye, G.F. Nellis, S.A. Klein, Comparison of CFD analysis to empirical data in a commercial vortex tube, Int. J. Refrig. 29 (2006) 71–80

[14] S. Akhesmeh, N. Pourmahmoud, H. Sedgi, Numerical study of the temperature separation in the Ranque-Hilsch vortex tube, Am. J. Eng. Appl. Sci. 1 (2008) 181–187

[15] R. Shamsoddini, A.H. Nejad, Numerical analysis of the effects of nozzles number on the flow and power of cooling of a vortex tube, Int. J. Refrig. 33 (2010) 774–782

[16] R. Shamsoddini, A. Fighih-Khorasani, A new approach to study and optimize cooling performance of a Ranque-Hilsch vortex tube, Int. J. Refrig. 33 (2012) 2339–2348

[17] A. Bramo, N. Pourmahmoud, Computational fluid dynamics simulation of length to diameter ratio effects on the energy separation in a vortex tube, Thermal Sci. 15 (2011) 833–848

[18] N. Pourmahmoud, A. Hasanzadeh, O. Moutaby, Numerical analysis of the effect of helical nozzles gap on the cooling capacity of Ranque-Hilsch vortex tube, Int. J. Refrig. 35 (2012) 1473–1483

[19] M. Avci, The effects of nozzle aspect ratio and nozzle number on the performance of the Ranque-Hilsch vortex tube, Appl. Thermal Eng. 50 (2013) 302–308

[20] H. Takahama, H. Yokosawa, Energy separation in vortex tubes with a divergent chamber, J. Heat Transfer 103 (1981) 196–203